

Intrinsic valley-polarized quantum anomalous Hall effect in a two-dimensional germanene/MnI_2 van der Waals heterostructure

Xiao-Jing Dong(董晓晶) and Chang-Wen Zhang(张昌文)

Citation: Chin. Phys. B, 2024, 33 (**7**): 077303. DOI: 10.1088/1674-1056/ad4bbd
Journal homepage: http://cpb.iphy.ac.cn; http://iopscience.iop.org/cpb

What follows is a list of articles you may be interested in

Recent progress on valley polarization and valley-polarized topological states in two-dimensional materials

Fei Wang(王斐), Yaling Zhang(张亚玲), Wenjia Yang(杨文佳), Huisheng Zhang(张会生), and Xiaohong Xu(许小红)
Chin. Phys. B, 2024, 33 (**1**): 017306. DOI: 10.1088/1674-1056/ad0713

Low-damage photolithography for magnetically doped $(Bi,Sb)_2Te_3$ quantum anomalous Hall thin films

Zhiting Gao(高志廷), Minghua Guo(郭明华), Zichen Lian(连梓臣), Yaoxin Li(李耀鑫), Yunhe Bai(白云鹤), Xiao Feng(冯硝), Ke He(何珂), Yayu Wang(王亚愚), Chang Liu(刘畅), and Jinsong Zhang(张金松)
Chin. Phys. B, 2023, 32 (**11**): 117303. DOI: 10.1088/1674-1056/ad0147

Spin- and valley-polarized Goos-Hänchen-like shift in ferromagnetic mass graphene junction with circularly polarized light

Mei-Rong Liu(刘美荣), Zheng-Fang Liu(刘正方), Ruo-Long Zhang(张若龙), Xian-Bo Xiao(肖贤波), and Qing-Ping Wu(伍清萍)
Chin. Phys. B, 2023, 32 (**3**): 037301. DOI: 10.1088/1674-1056/ac89e2

Current carrying states in the disordered quantum anomalous Hall effect

Yi-Ming Dai(戴镒明), Si-Si Wang(王思思), Yan Yu(禹言), Ji-Huan Guan(关济寰), Hui-Hui Wang(王慧慧), and Yan-Yang Zhang(张艳阳)
Chin. Phys. B, 2022, 31 (**9**): 097302. DOI: 10.1088/1674-1056/ac5d2b

Improvement of valley splitting and valley injection efficiency for graphene/ferromagnet heterostructure

Longxiang Xu(徐龙翔), Wengang Lu(吕文刚), Chen Hu(胡晨), Qixun Guo(郭奇勋), Shuai Shang(尚帅), Xiulan Xu(徐秀兰), Guanghua Yu(于广华), Yu Yan(岩雨), Lihua Wang(王立华), Jiao Teng(滕蛟)
Chin. Phys. B, 2020, 29 (**7**): 077304. DOI: 10.1088/1674-1056/ab8db2

SPECIAL TOPIC — Valleytronics

Intrinsic valley-polarized quantum anomalous Hall effect in a two-dimensional germanene/MnI_2 van der Waals heterostructure

Xiao-Jing Dong(董晓晶)[1,2] and Chang-Wen Zhang(张昌文)[1,†]

[1] *School of Physics and Technology, Institute of Spintronics, University of Jinan, Jinan* 250022, *China*
[2] *School of Physics and Physical Engineering, Qufu Normal University, Qufu* 273100, *China*

(Received 31 January 2024; revised manuscript received 24 April 2024; accepted manuscript online 15 May 2024)

Valley-polarized quantum anomalous Hall effect (VQAHE), combined nontrivial band topology with valleytronics, is of importance for both fundamental sciences and emerging applications. However, the experimental realization of this property is challenging. Here, by using first-principles calculations and modal analysis, we predict a mechanism of producing VQAHE in two-dimensional ferromagnetic van der Waals germanene/MnI_2 heterostructure. This heterostructure exhibits both valley anomalous Hall effect and VQAHE due to the joint effects of magnetic exchange effect and spin–orbital coupling with the aid of anomalous Hall conductance and chiral edge state. Moreover interestingly, through the electrical modulation of ferroelectric polarization state in In_2Se_3, the germanene/MnI_2/In_2Se_3 heterostructure can undergo reversible switching from a semiconductor to a metallic behavior. This work offers a guiding advancement for searching for VQAHE in ferromagnetic van der Waals heterostructures and exploiting energy-efficient devices based on the VQAHE.

Keywords: valley-polarized, quantum anomalous Hall effect, ferromagnetic

PACS: 73.43.–f, 73.22.–f, 71.15.Mb, 79.60.Jv **DOI:** 10.1088/1674-1056/ad4bbd

1. Introduction

Valley, another degree of freedom of carriers analogous to spin and charge, has attracted widespread interest since it uniquely combines low energy consumption and high storage density,[1–3] which is characterized by the energy extrema on the valence/conduction band.[4–8] In recent years, new phases of matter have emerged from the coupling of two-dimensional (2D) hexagonal lattices to them due to experimental discoveries of valleytronic materials such as 2D graphene and transition metal dichalcogenides (TMDs). A defining characteristic of this coupling is the valley Hall effect (VHE), which is determined by its intrinsic inversion ($\mathcal{P}$) symmetry breaking.[9,10] Graphene loses its VHE and valley-dependent optical selection rule since it crystallizes in an $\mathcal{P}$-symmetric honeycomb lattice.[11] In this regard, germanene is an ideal valley material to achieve valley-dependent property owing to its intrinsic $\mathcal{P}$-symmetry breaking.[12] VHE links Berry curvature with $\mathcal{P}$-symmetry broken related valley degree, which produces a transverse Hall current due to carriers moving in opposite directions under an in-plane (IP) electric field. Physically, time reversal ($\mathcal{T}$) symmetry is also an important factor for various Hall effects. Quantum spin Hall effect (QSHE), for instance, is topologically protected due to its $\mathcal{T}$-symmetry.[13] The quantum anomalous Hall effect (QAHE) occurs when the $\mathcal{T}$-symmetry is broken with magnetic doping.[14] Valley-polarized quantum anomalous Hall effect (VQAHE) combines valleytronics and spintronics with nontrivial band topology.[15–17] Removing the $\mathcal{T}$-symmetry to generate VQAHE is a pressing issue. Several alternative methods have been proposed to achieve VQAHE, such as decorating magnetic transition metal atoms,[18] statically magnetic field,[19] optical pumping,[20] and magnetic proximity effects.[21,22] Evidently, to overcome this difficulty, one must go beyond the existing paradigm to generate the VQAHE.

Recently, the approach of magnetic proximity effects in ferromagnetic (FM) van der Waals (vdW) heterostructures (HTSs) is the most attractive and effective way to lift the valley degeneracy.[23–25] In particular, the vdW HTS composed of 2D layered materials offers a promising approach to minimize lattice mismatch, thereby providing multiple opportunities for manipulating the valley splitting through the utilization of diverse magnetic substrates.[22] With the development of growth technology for 2D intrinsic FM materials, for example, $Gr_2Ge_2Te_6$,[26] VS_2,[27] CrI_3,[28] $MoTe_2$/EuO(111),[29,30] an attractive opportunity for seeking the combination of valleytronics and band topology into FM vdW HTSs likely triggers emerging physics and novel applications.

Here, with the aid of magnetic exchange effect, we propose that germanene/MnI_2 HTS can realize valley-dependent topological phase. We can see that the contrasting valley features responses to K/K' valleys in spin splitting with the $\mathcal{P}$-symmetry broken. Furthermore, with introduction of the magnetic proximity effect of an FM substrate, the valley-splitting in K valley still preserves the trivial feature, while the bands in K' valley undergo a band inversion phenomenon and then become a nontrivial phase. With first-principles

†Corresponding author. E-mail: ss_zhangchw@ujn.edu.cn

© 2024 Chinese Physical Society and IOP Publishing Ltd

supports, germanene/MnI_2 HTS favors out-of-plane (OOP) magnetization and possesses both QAHE and anomalous valley Hall effect (AVHE) in nature. Herein, VQAHE with a valley-dependent chiral edge state could enrich valley-related physics.

2. Computational methods

Our first-principles calculations are performed using Vienna *ab initio* simulation package (VASP)[31,32] based on the density functional theory (DFT). The electronic structure is described by the projector augmented wave (PAW) potentials.[33] The generalized gradient approximation (GGA) in the form of Perdew–Burke–Ernzerhof (PBE)[32] is adopted for the exchange–correlation. The force and energy convergence criteria are 10^{-3} eV/Å and 10^{-6} eV, respectively. The energy cutoff of the plane wave basis set is 500 eV. A Monkhorst–Pack grid of $15\times15\times1$ is adopted to sample the Brillouin zone (BZ) and a grid of $25\times25\times1$ is used for magnetic anisotropy energy (MAE) calculation. A vacuum space of 25 Å is adopted to avoid interactions between adjacent layers. The vdW corrected functional Grimme (DFT-D3) method is employed.[34] PBE$+U$ method is adopted and $U=4.0$ eV due to the correlation effects of Mn-3d electrons, as previously reported.[35–37] We construct a maximally localized Wannier (MLWF) function by the WANNIER90 package[38] based on the band structures in the presence of SOC calculated by using DFT. The chiral edge states and anomalous Hall conductivity (AHC) are calculated by the iterative Greens method as implemented in the WannierTools.[39]

3. Results and discussion

Here, we construct an FM vdW HTS by depositing the monolayer (ML) germanene onto a MnI_2 substrate. The electronic and topological properties resulting from magnetic exchange interactions in germane/MnI_2 FM vdW HTS are elucidated through first principles calculations. Figure S1 presents the crystal structures of ML-germanene and FM ML-MnI_2 and their electronic band structures. As demonstrated in experiments, some bulk metal dihalides possess a naturally layered structure.[40] Thus, akin to MoS_2 and WSe_2, individual layers of dihalides can potentially be extracted from the bulk through exfoliation techniques. We optimize all atomic positions and lattice constants to ensure the minimum-energy structure for each ML. The structure of ML-dihalides bears conceptual resemblance to that of well-established TMDs. Each metal dihalide consists of three atomic layers, specifically the Mn atom layer sandwiched between two I atom layers. Namely, six I atoms encompass the Mn atom to form an octahedral $[MnI_6]^{4-}$ unit with each Mn ion possessing $5\mu_B$ magnetic moment.[35] Three possible configurations are considered, as shown in Fig. S2 and the lattice mismatch is 3.63% by the formula $\eta=\frac{|a_1-a_2|}{(a_1+a_2)/2}\times100\%$.

Subsequently, the stability of germanene/MnI_2 HTS is assessed by binding energy, and its charge transfer mechanism is investigated. To evaluate the stability of germanene/MnI_2 HTS, we define $E_b=E_{HTS}-E_{germanene}-E_{MnI_2}$, where E_{HTS}, $E_{germanene}$, and E_{MnI_2} are the total energies of germanene/MnI_2 HTS, ML-germanene, ML-MnI_2, respectively. The findings of E_b (refer to Table S1) indicate that all configurations of germanene/MnI_2 HTS under consideration are experimentally viable. Grmanene/MnI_2 HTS features an interlayer distance of approximately 3.6 Å, which exceeds the sum of the covalent radii of I atom (1.33 Å) and Ge atom (1.22 Å). This discrepancy suggests a lack of chemical bonding between the layers, exhibiting typical vdW interaction in germanene/MnI_2 HTS.[41] Hence, we will utilize the most stable structure C–I, as shown in Figs. 1(a) and 1(b), as a representative example to further investigate the physical properties of germanene/MnI_2 FM vdW HTS in subsequent calculations.

Subsequently, our focus shifts towards the magnetic properties of germanene/MnI_2 HTS based on the C–I structure. In order to determine the magnetic ground state, we consider two collinear magnetic configurations within a $2\times2\times1$ supercell, encompassing both an FM state and three antiferromagnetic (AFM) states as illustrated in Fig. S3. This result demonstrates the superior energetic favorability of the FM configuration over the AFM configuration in the germane/MnI_2 HTS. Specifically, FM configuration exhibits a 1.4 meV per formula unit (f.u.$^{-1}$) lower energy compared to AFM1 and a 1.3 meV·f.u.$^{-1}$ lower energy compared to both AFM2 and AFM3 configurations, highlighting the enhanced preference for FM coupling. The FM state of germanene/MnI_2 HTS is closely linked to its geometric structure. The estimated bond angle between I–Mn–I is 88.6°, which is close to 90.0°. According to the Goodenough–Kanamori–Anderson rules,[42] this structure would favor FM coupling due to super-exchange interactions mediated by neighboring Mn atoms through the I atom. When germanene/MnI_2 HTS is formed, two electrons are transferred from one Mn atom to the six neighboring I atoms. As a result, Mn^{2+} adopts an electronic state of $3d^5$. This leads to the half-filled $3d^5$ orbitals contributing to a formal magnetic moment of $5\mu_B$ on each Mn atom. Additionally, our DFT calculations validate the presence of a spontaneous spin-polarized state in germanene/MnI_2 HTS, exhibiting a magnetic moment of $5\mu_B$ per unit cell. Furthermore, the magnetism in the FM ground state is predominantly contributed by the Mn atoms.

In light of the Mermin–Wagner theorem,[43] strong thermal fluctuations can easily disrupt long-range ferromagnetic ordering in low-dimensional systems at finite temperatures. However, the recent discovery of 2D magnetic ma-

terial $Cr_2Ge_2Te_6$[44] reveals that magnetic anisotropy energy (MAE), primarily influenced by the SOC effect, plays an important role in maintaining the magnetic ordering stability. A larger MAE indicates a stronger resistance to thermal fluctuations in magnetic ordering, which can enhance data storage performance.[10] The MAE, defined as the energy difference $E_{\mathrm{MAE}} = E_{\text{in-plane}} - E_{\text{out-of-plane}}$ between in-plane (IP) and out-of-plane (OOP) magnetization directions, incorporates the effect of SOC. A positive or negative MAE signifies an easy magnetization axis aligned with either OOP or IP orientation. In this work, the MAE of germanene/MnI_2 HTS is calculated to be $E_{\mathrm{MAE}} = -14$ μeV. Hence, this system can be regarded as a 2D XY magnet due to the above elucidation, wherein manipulation of the magnetization from in-plane to OOP orientation is achieved by surpassing an energy barrier of 14 μeV, thereby resulting in a valley polarization.

In order to elucidate the charge transfer mechanism between the ML-germanene and MnI_2 layers, we further perform the work functions, Bader charge analysis and differential charge density of germanene/MnI_2 HTS. The work function is defined as the energy difference between the vacuum level and the Fermi level (E_F). As shown in Figs. 1(d)–1(f), the work functions of ML-germanene, ML-MnI_2, germanene/MnI_2 HTS are 4.48 eV, 5.84 eV, and 4.63 eV, respectively. The lower work function of ML-germanene, compared with that of ML-MnI_2, shows the possibility of electron flow from ML-germanene to ML-MnI_2 upon their contact in Fig. 1(c). Consequently, the ML-MnI_2 acquires positive charges while the ML-germanene gathers negative charges. Additionally, the work function of the germanene/MnI_2 FM HTS lies between those of ML-germanene and ML-MnI_2 owing to spontaneous charge transfer between the two layers. This results in a balanced work function achieved by lifting E_F of ML-germanene and ML-MnI_2 up and down, respectively. In Fig. 1(f), we present the 3D differential charge density of HTS to directly observe the charge transfer occurring at its interface. The cyan and yellow regions represent electron depletion and accumulation, respectively, indicating the spontaneous flow of electrons from the ML-germanene layer to the adjacent ML-MnI_2 layer. Consequently, a vertical built-in electric field forms at the interface, pointing from the germanene layer towards the MnI_2 layer. The presence of the built-in electric field impedes the spontaneous diffusion of holes and electrons yielded by the work function difference, which results in a dynamic balance at the interface. Besides, Bader charge analysis is conducted in germanene/MnI_2 FM HTS, revealing that 0.122 electrons are transferred from the germanene layer to the MnI_2 layer. Aligned with theoretical results from other HTSs, such as stanene/CrI_3[41] and germanene/NiI_2,[45] these findings confirm the interlayer charge transfer in the germanene/MnI_2 HTS through various methods, thus supporting the accuracy of our results.

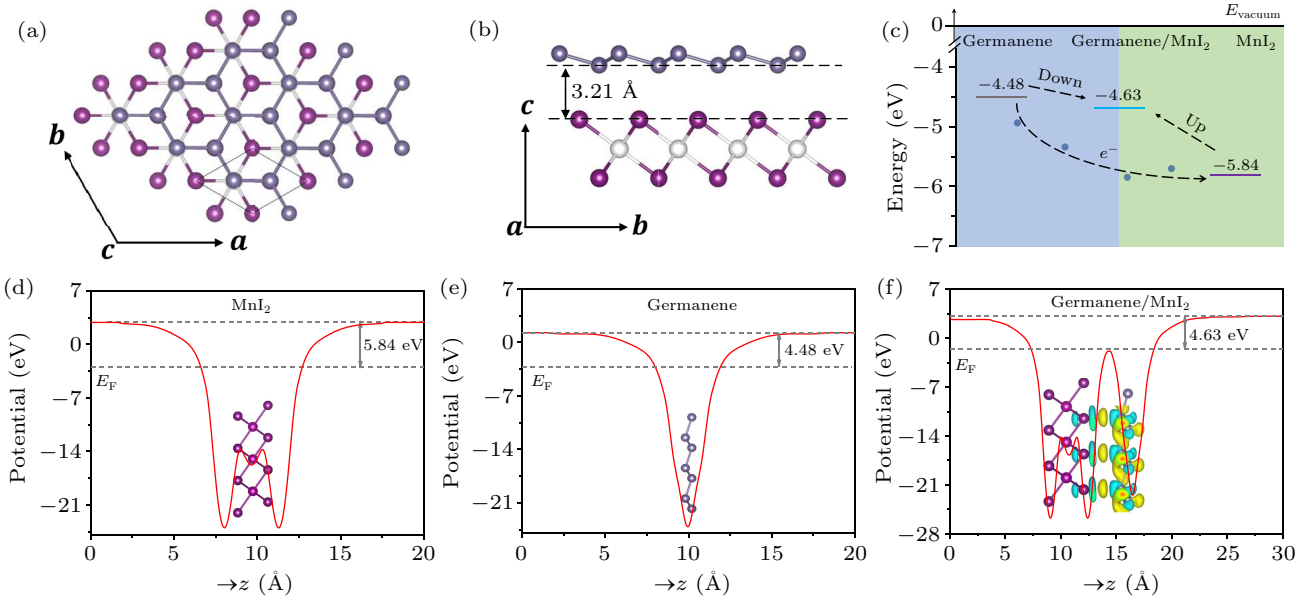


Fig. 1. Top (a) and side (b) views of germanene/MnI_2 HTS. (c) The transfer direction of electrons and the movement of the Fermi level during HTS formation. The electrostatic potentials of ML-MnI_2 (d), ML-germanene (e) and germanene/MnI_2 FM HTS (f). The charge density difference is presents in (f), while the regions highlighted in cyan and yellow correspond to electron depletion and accumulation, respectively.

Next, we mainly focus on the valley polarization properties of germanene/MnI_2 FM vdW HTS. The germanene/MnI_2 HTS shows semiconducting characteristics with a direct bandgap of 44.3 meV in Fig. 2(a). Upon inclusion of SOC, the removal of valley degeneracy is observed due to broken $\mathcal{T}$-symmetry. It can be seen that obvious valley polarization occurs at the valence band maximum (VBM) and the conduction band minimum (CBM). As shown in Fig. 2(b), the band struc-

tures of the valley-polarized states reveal that the K/K' valleys in VBM exhibit the opposite spin channels and unequal energy values. Specifically, the presence of the magnetic substrate disrupts $\mathcal{T}$-symmetry by means of the magnetic proximity effect, thereby inducing valley polarization similar to that observed in van der Waals heterostructures based on TMD and FM substrates. For the sake of convenience, the degree of valley polarization can be denoted as $\Delta E_{\rm val} = |E_K - E_{K'}|$ and $\Delta E_{\rm con} = |E_K - E_{K'}|$, where they represent the energy level difference between K/K' points at the VBM and CBM. If the magnetization is oriented towards the $+z$ direction, the valley polarization originating from the spin-down channel can reach up to 12.4 meV in CBM and 5.8 meV in VBM. By examining the orbital-resolved band structures with SOC in Fig. 2(c), we observe that the states near the $E_{\rm F}$ are predominantly contributed by Ge_1-p_z and Ge_2-p_z orbitals. This suggests the existence of hybridization and charge transfer between the germanene and MnI_2 layers.

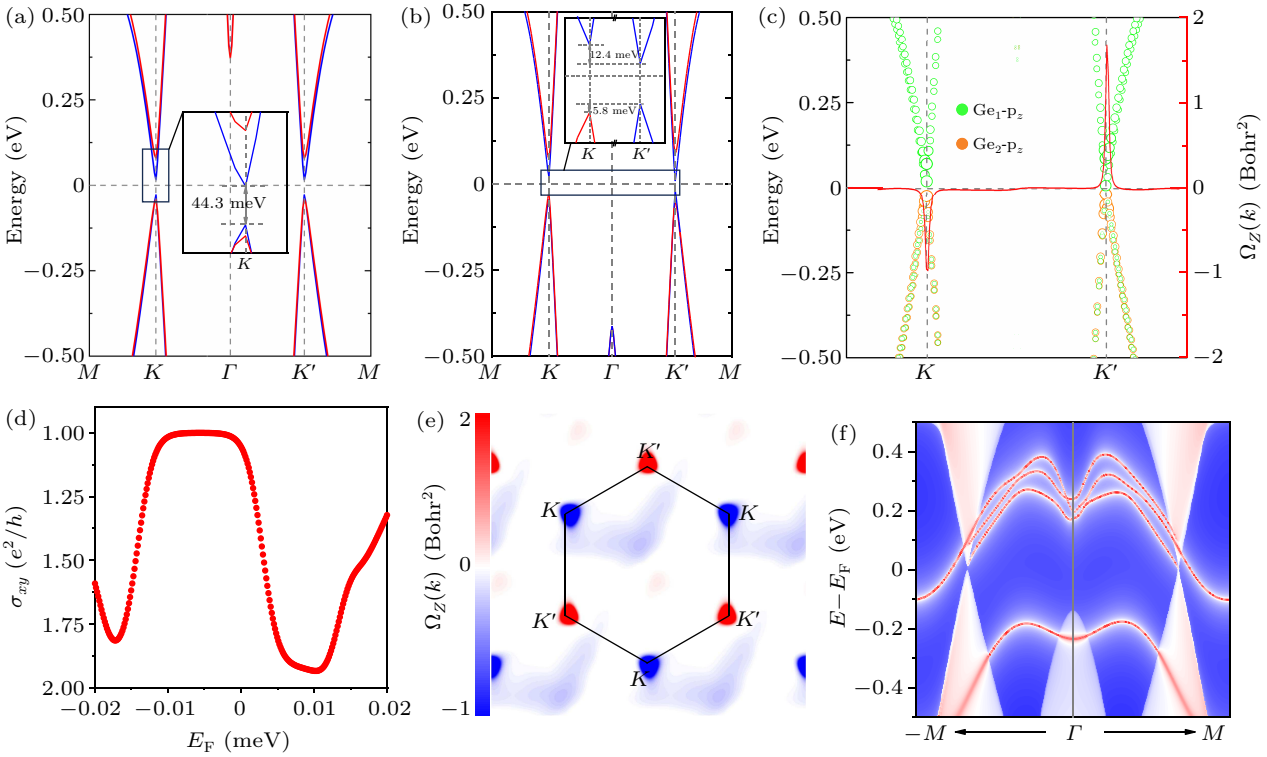


Fig. 2. Spin-resolved band structures of germanene/NiI_2 HTS (a) without and (b) with SOC. The solid red and blue lines represent the spin up and spin down channels, respectively. (c) Orbital-resolved band structures of germanene/NiI_2 HTS. The green circle represents the element projection of Ge_1-p_z, whereas the orange circle represents the element projection of Ge_2-p_z. (d) Anomalous Hall conductance σ_{xy}. (e) Distribution of Berry curvature within the first BZ. (f) Edge state of germanene/NiI_2 HTS.

To verify this conjecture, we then establish the Wannier-function-based tight-binding (WFTB) model by utilizing the generated Wannier functions including SOC. The Hamiltonian of WFTB with SOC can be written as[46,47]

$$H_{{\rm SOC},\alpha\beta}(\boldsymbol{k}) = \langle \psi_{\boldsymbol{k},\alpha} | H_{\rm SOC} | \psi_{\boldsymbol{k},\beta} \rangle = \sum_{\boldsymbol{R}} {\rm e}^{{\rm i}\boldsymbol{k}\cdot\boldsymbol{R}} t_{\alpha\beta}(\boldsymbol{R}-0), \quad (1)$$

$$t_{\alpha\beta}(\boldsymbol{R}-0) = \langle \boldsymbol{0}+\boldsymbol{s}_\alpha | H_{\rm SOC} | \boldsymbol{R}+\boldsymbol{s}_\beta \rangle, \quad (2)$$

where $|\psi_{\boldsymbol{k}}\rangle$ and $\boldsymbol{R}$ represent the Bloch states over the BZ and the Bravais lattice vector. The hopping parameters $t_{\alpha\beta}(\boldsymbol{R}-0)$ represent the transition from orbital β located at site $\boldsymbol{s}_\beta$ in the home cell at $\boldsymbol{R}=0$ to orbital α situated at sites $\boldsymbol{s}_\alpha$ in the unit cell positioned at $\boldsymbol{R}$. Next, the Zeeman exchange energy ($E_{\rm exc}$) can be expressed as $E_{\rm exc} = g\mu_{\rm B}\boldsymbol{B}$, where g is the effective g factor and $\boldsymbol{B}$ is the magnetic field strength. It should be noted that the Peierls phase in the hopping parameters $t_{\alpha\beta}$ or Landau levels is disregarded here. The method is deemed reliable and effective for investigating the topological states induced by an FM substrate.

A vital characteristic for distinguishing between K/K' valleys in germanene/MnI_2 FM HTS without inversion symmetry is the presence of valley-contrasting Berry curvature, which can be computed as[48,49]

$$\Omega(\boldsymbol{k}) = \sum_n f_n \Omega_n(\boldsymbol{k}), \quad (3)$$

$$\Omega_n(\boldsymbol{k}) = -2{\rm Im} \sum_{m\neq n} \frac{\hbar^2 \langle \psi_{n\boldsymbol{k}} | \upsilon_x | \psi_{m\boldsymbol{k}} \rangle \langle \psi_{m\boldsymbol{k}} | \upsilon_y | \psi_{n\boldsymbol{k}} \rangle}{(E_m - E_n)^2}. \quad (4)$$

Here, the sum is over all occupied contributions. f_n is a function of Fermi–Dirac distribution, $\upsilon_{x(y)}$ represents the velocity operator in the x (y) direction. $\langle \psi_{n\boldsymbol{k}}|$ and $|\psi_{m\boldsymbol{k}}\rangle$ are the Bloch wave functions with eigenvalues E_n and E_m. Next, we validate the feasibility of realizing VQAHE in the germanene/MnI_2 HTS by calculating the Berry curvature. As illustrated in

Fig. 2(e), it is observed that the Berry curvatures of the K valley and K' valley exhibit unequal magnitudes and opposite signs, indicating that the flow of electrons occurs within a curled field and contributes to the quantized Hall conductance. The Chern number C is calculated to be -1, which is also obtained by integrating the Berry curvature in the whole BZ. It is noteworthy that the C solely originates from the K' valley , that is, $C_{K'} = 1$ and $C_K = 0$, resulting in a valley Chern number $C_\upsilon = C_K - C_{K'} = -1$ and so indicating the realization of VQAHE. The non-zero valley Chern number C_υ of germanene/MnI_2 HTS confirms the existence of topologically nontrivial edge states and quantized Hall conductivity. Thus, we utilize the iterative Green's function method based on the WFTB Hamiltonian to compute the edge states, which is plotted in Fig. 2(f). It is evident that a topological chiral edge state connects the valence and conduction bands, indicating the presence of a quantum anomalous Hall phase. Next, we employ the WFTB Hamiltonian based on Kubo formula to calculate the anomalous Hall conductance (AHC) σ_{xy} as depicted in Fig. 2(d). σ_{xy} shows a quantized plateau of $\sigma_{xy} = -e^2/h$ inside the nontrivial band gap.

Nowadays, electrical manipulation of magnetism is a topic of significant interest for spintronic applications that prioritize low energy consumption. To validate the aforementioned concept, an additional layer of In_2Se_3 is introduced at the bottom of germanene/MnI_2 HTS, resulting in a multiferroic vdW HTS term as germanene/MnI_2/In_2Se_3. Here, two distinct polar configurations are considered for the In_2Se_3 layer: either both ferroelectric layers are oriented upwards ($P\uparrow$) or downwards ($P\downarrow$). Figures 3(a) and 3(c) illustrate the geometric arrangements of germanene/MnI_2/In_2Se_3 in the $P\uparrow$ and $P\downarrow$ configurations. For $P\uparrow$ cases, characterized by a direct band gap of 0.57 eV, the germane/MnI_2/In_2Se_3 HTS keeps a semiconducting nature as depicted in Fig. 3(b). By inducing a flip in the electrical polarization of In_2Se_3, we observe an upward shift in the bands associated with the germanene/MnI_2 HTS, resulting in their intersection at the E_F. This indicates that fascinating metallic properties are generated by the germane/MnI_2/In_2Se_3 HTS, as depicted in Fig. 3(d). From the band structure, it can be seen that the electronic states of the E_F layer are predominantly contributed by the germanene/MnI_2 layer, thereby imparting metallic properties to germanene/MnI_2/In_2Se_3 HTS. Consequently, when subjected to an upward ferroelectric polarization of In_2Se_3, it becomes feasible to generate a complete polarization current. Therefore, by reversing the polarization orientation of the ML-In_2Se_3 from upward to downward, a transition can be induced in the germanene/MnI_2 system, transforming it from a semiconductor into a metal. Notably, this process leads to a significant change in the material's properties. The energy barrier for the transition from $P\uparrow$ configuration to $P\downarrow$ configuration is 44.8 eV. Therefore, the germanene/MnI_2/In_2Se_3 HTS offers sufficient bistability for the device application.

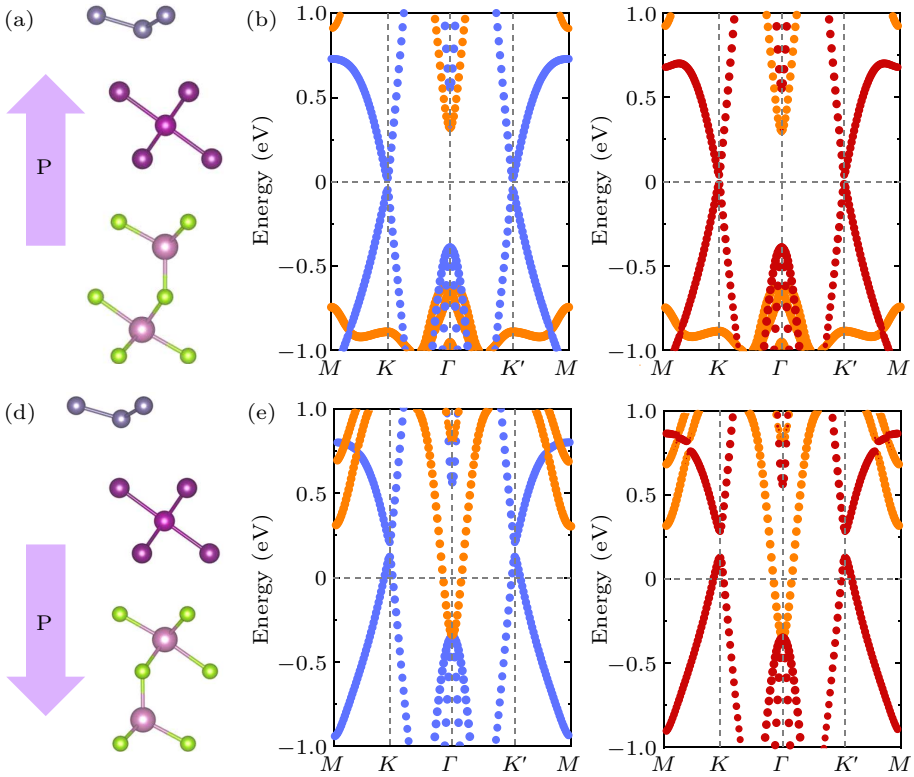


Fig. 3. Structural diagrams of germanene/MnI_2/In_2Se_3 HTS in the $P\uparrow$ (a) and $P\downarrow$ (c) states along the z direction. Calculated band structures in the $P\uparrow$ (b) and $P\downarrow$ (d) states. The red and blue circles in the band structure correspond to spin-up and spin-down states of germanene/MnI_2 HTS, respectively. The orange circle denotes the components of In_2Se_3.

4. Summary

In conclusion, we explain a mechanism of VQAHE in FM hexagonal lattice based on first-principles calculations. We further systematically study topological phase transitions and valley-based Hall effects in germanene/MnI_2 HTS. More interesting, we have designed vdW HTS comprising FM germanene/MnI_2 HTS and ferroelectric In_2Se_3 monolayers with multiferroic properties. Reversing the direction of ferroelectric polarization of In_2Se_3 induces a transition in germanene/MnI_2/In_2Se_3 HTS, transforming it from a semiconductor into a metal. The intriguing phenomenon can be primarily ascribed to the charge transfer occurring between the germanene/MnI_2 HTS and ML-In_2Se_3. The present work aims to achieve nonvolatile electrical control of metallicity, thereby paving the way for the development of interfacial magnetoelectric physics and applications.

Acknowledgments

Project supported by the National Natural Science Foundation of China (Grant No. 52173283), Taishan Scholar Program of Shandong Province (Grant No. ts20190939), and Independent Cultivation Program of Innovation Team of Jinan City (Grant No. 2021GXRC043).

References

[1] Wang W G, Li M, Hageman S and Chien C L 2012 *Nat. Mater.* **11** 64
[2] Tsymbal E Y 2012 *Nat. Mater.* **11** 12
[3] Maruyama T, Shiota Y, Nozaki T, Ohta K, Toda N, Mizuguchi M, Tulapurkar A A, Shinjo T, Shiraishi M, Mizukami S, Ando Y and Suzuki Y 2009 *Nat. Nanotechnol.* **4** 158
[4] Jia K, Dong X J, Li S S, Ji W X and Zhang C W 2023 *Nanoscale* **15** 8395
[5] Jia K, Dong X J, Li S S, Ji W X and Zhang C W 2023 *J. Mater. Chem. C* **11** 10359
[6] Zhang A, Yang K, Zhang Y, Pan A and Chen M 2021 *Phys. Rev. B* **104** L201403
[7] Aivazian G, Gong Z, Jones A M, Chu R L, Yan J, Mandrus D G, Zhang C, Cobden D, Yao W and Xu X 2015 *Nat. Phys.* **11** 148
[8] Liu Y, Gao Y, Zhang S, He J, Yu J and Liu Z 2019 *Nano Res.* **12** 2695
[9] Olsen T and Souza I 2015 *Phys. Rev. B* **92** 125146
[10] Tong W, Gong S, Wan X and Duan C 2016 *Nat. Commun.* **7** 13612
[11] Jiang Y, Low T, Chang K, Katsnelson M I and Guinea F 2013 *Phys. Rev. Lett.* **110** 046601
[12] Chen M X, Zhong Z and Weinert M 2016 *Phys. Rev. B* **94** 075409
[13] Kane C L and Mele E J 2005 *Phys. Rev. Lett.* **95** 226801
[14] Liu C X, Qi X L, Dai X, Fang Z and Zhang S C 2008 *Phys. Rev. Lett.* **101** 146802
[15] Wu B, Song Y L, Ji W X, Wang P J, Zhang S F and Zhang C W 2023 *Phys. Rev. B* **107** 214419
[16] He R, Wang D, Luo N, Zeng J, Chen K Q and Tang L M 2023 *Phys. Rev. Lett.* **130** 046401
[17] Sun H, Li S S, Ji W X and Zhang C W 2022 *Phys. Rev. B* **105** 195112
[18] Zhou J, Sun Q and Jena P 2017 *Phys. Rev. Lett.* **119** 046403
[19] Li Y, Liu Y, Wang C, Wang J, Xu Y and Duan W 2018 *Phys. Rev. B* **98** 201407
[20] Macneill D, Heikes C, Mak K F, Anderson Z, Kormányos A, Zólyomi V, Park J and Ralph D C 2015 *Phys. Rev. Lett.* **114** 037401
[21] Zeng M, Xiao Y, Liu J, Yang K and Fu L 2018 *Chem. Rev.* **118** 6236
[22] Liu Y, Guo J, Zhu E, Liao L, Lee S J, Ding M, Shakir I, Gambin V, Huang Y and Duan X 2018 *Nature* **557** 696
[23] Qi J, Li X, Niu Q and Feng J 2015 *Phys. Rev. B* **92** 121403
[24] Hu T, Zhao G, Gao H, Wu Y, Hong J, Stroppa A and Ren W 2020 *Phys. Rev. B* **101** 125401
[25] Seyler K L, Zhong D, Huang B, Linpeng X, Wilson N P, Taniguchi T, Watanabe K, Yao W, Xiao D, McGuire M A, Fu K M C and Xu X 2018 *Nano Lett.* **18** 3823
[26] Liu W R, Dong X J, Lv Y Z, Ji W X, Cao Q, Wang P J, Li F and Zhang C W 2022 *Nanoscale* **14** 3632
[27] Lei C, Li X, Ma Y and Qian Z 2023 *Phys. Rev. B* **108** 155431
[28] Huang B, Clark G, Navarro-Moratalla E, Klein D R, Cheng R, Seyler K L, Zhong Di, Schmidgall E, McGuire M A, Cobden D H, Yao W, Xiao D, Jarillo-Herrero P and Xu X 2017 *Nature* **546** 270
[29] Zhang A, Gong Z, Zhu Z, Pan A and Chen M 2020 *Phys. Rev. B* **102** 155413
[30] Zhang Q, Yang S A, Mi W, Cheng Y and Schwingenschlögl U 2016 *Adv. Mater.* **28** 959
[31] Kresse G, Furthmüller J and Hafner J 1994 *Phys. Rev. B* **50** 13181
[32] Perdew J P, Burke K and Ernzerhof M 1996 *Phys. Rev. Lett.* **77** 3865
[33] Kresse G and Joubert D 1999 *Phys. Rev. B* **59** 1758
[34] Allouche A 2012 *J. Comput. Chem.* **32** 174
[35] Wu X, Cai Y, Xie Q, Weng H, Fan H and Hu J 2012 *Phys. Rev. B* **86** 134413
[36] Yekta Y, Hadipour H, Şaşloglu E, Friedrich C, Jafari S A, Blügel S and Mertig I 2021 *Phys. Rev. Mater.* **5** 034001
[37] Bo X, Fu L, Wan X, Li S and Pu Y 2024 *Phys. Rev. B* **109** 014405
[38] Marzari N, Mostofi A A, Yates J R, Souza I and Vanderbilt D 2012 *Rev. Mod. Phys.* **84** 1419
[39] Wu Q S, Zhang S N, Song H F, Troyer M and Soluyanov A A 2018 *Comput. Phys. Commun.* **224** 405
[40] Botana A S and Norman M R 2019 *Phys. Rev. Mater.* **3** 044001
[41] Zhai B, Du J, Shen C, Wang T, Peng Y, Zhang Q and Xia C 2019 *Phys. Rev. B* **100** 195307
[42] Anderson P W 1959 *Phys. Rev.* **115** 2
[43] Mermin N D and Wagner H 1966 *Phys. Rev. Lett.* **17** 1133
[44] Gong C, Li L, Li Z, Ji H, Stern A, Xia Y, Cao T, Bao W, Wang C, Wang Y, Qiu Z Q, Cava R J, Louie S G, Xia J and Zhang X 2017 *Nature* **546** 265
[45] Dong X J, Ren M J and Zhang C W 2022 *Phys. Chem. Chem. Phys.* **24** 21631
[46] Choi Y, Villanova J W and Park K 2020 *Phys. Rev. B* **101** 035105
[47] Villanova J W and Park K 2018 *Phys. Rev. B* **98** 075123
[48] Thouless D J, Kohmoto M, Nightingale M P and den Nijs M 1982 *Phys. Rev. Lett.* **49** 405
[49] Yao Y, Kleinman L, MacDonald A H, Sinova J, Jungwirth T, Wang D S, Wang E and Niu Q 2004 *Phys. Rev. Lett.* **92** 037204